Supporting Information

Atomic Resolution Insights into the Structural Aggregations and Optical Properties of the Neat Imidazolium Based Ionic Liquid

Likai Du[*,†,‡,#], *Cuihuan Geng*[‡], *Dongju Zhang*[*,‡], *Zhenggang Lan*[*,†], *Chengbu Liu*[b]

[†] *Key Laboratory of Biobased Materials, Qingdao Institute of Bioenergy and Bioprocess Technology, Chinese Academy of Sciences, Qingdao, 266101, Shandong, P. R. China. E-mail: lanzg@qibebt.ac.cn*

[‡]*Institute of Theoretical Chemistry, Shandong University, Jinan, 250100, P. R. China. E-mail: zhangdj@sdu.edu.cn*

[#]*Hubei Key Laboratory of Agricultural Bioinformatics, College of Informatics, Huazhong Agricultural University, Wuhan, 430070, P.R. China. E-mail: dulikai@mail.hzau.edu.cn*

1. Technical details of the computational methods

1.1 Classical molecule dynamics (MD) simulations

The systems contain 512 ion pairs, and the initial configuration was obtained by randomly disposing 512 ion pairs in a cubic box. The force field parameters of the [Bmim] cation were taken from a recent publication of Lopes and Pádua's works[1], which based on the OPLS-AA/AMBER force field[2,3]. And the force field parameters of the amino acid anions were taken from Zhou's work[4], which was a refined force filed based on AMBER. Good agreement between experimental and computed values of density and molar volume were obtained. For example, the obtained molar volume at 343.15K was 0.3260 nm^3, which is very close to the experimental value of 0.3209 nm^3.[5,6]

Firstly, the initial configurations were minimized and then they were relaxed in the NVE ensemble for a few MD steps (100 ps) to remove the possible overlapping. In our scheme, the system was equilibrated at higher temperatures for 2 ns, and cooled down step-wise[7] and again equilibrated for 2 ns. The temperatures we use were 600, 550, 500, 400 and 350 K in our simulation. After this, the system was equilibrated for 10 ns at 343.15K, and then data were collected every 10 time steps for 10 ns. The potential and the density were monitored in the production stage. Well-converged dynamic properties could be obtained from MD runs for about tens of nanoseconds at the working temperature.

The periodic boundary conditions were applied in the simulations. The leapfrog algorithm was adopted to integrate the motion equations with a time step of 1 fs. The temperature was maintained at 343.15 K by Berendsen thermostat and the pressure was controlled via Berendsen barostat[8] at 1 bar. Electrostatic interactions were treated with a particle mesh Ewald (PME) summation[9,10]. The long-range dispersion correction for the energy and pressure were applied. The LINCS algorithm[11] was utilized to constrain all bonds involving the hydrogen in the imidazolium cation as Lopes et al. did[1]. The classical MD simulations were performed with GROMACS 4.5 package[12].

The microscopic structures of the [Bmim][Gly] with the radial distribution

functions (RDFs) in Figure S3. For the RDF of anions around cations, the first peak locates at 6.0 Å. The RDF of cations around cations suggests a decaying oscillation character in this strong coupled system. In the anion-anion RDFs, two obvious solvent shells can be observed. Overall, at least for distances less than approximately 15 Å, the value of RDF is greater than unity, indicating that "mobile" ions are not randomly distributed over the simulation cell but form well-defined clusters[79]. The spatial distribution function (SDF) of anions and cations around cations was used to refine the structural picture and rationalize the possible aggregation. The anions distribution around cations exhibits larger amplitudes close to the imidazolium ring plane. And the location of the anions is also possible near the less polar alkyl groups. The cation-cation SDFs are found to locate mainly in the regions below and above both sides of the imidazolium ring plane, which is consistent with our optimized hydrogen bonded geometries (Figure S1). Overall, these results provide us some preliminary and fundamental understanding about their possible microscopic structural aggregations.

1.2 Exchange-correlation functionals in TD-DFT methods

In the benchmark study, the calculations were performed with all the optimized geometries in Figure S1. A set of commonly used exchange-correlation functionals were used, which represent different families: 1) the pure generalized gradient approximation (GGA) functional: PBE, BLYP, PW91, HCTH407, B97D; 2) hybrid GGA functional: B3LYP, B3P86, B3PW91, PBE1PBE, X3LYP, mPW1PW91, mPW3PBE, mPW1PBE, BHandHLYP, HSE06, B1B95; 3) the meta-GGA and its hybrid functional: M06L, M11L, TPSS, tHCTH, TPSSh, tHCTHhyb, M05, M052X, M06, M062X, M06HF, BMK; 4) the range separated functionals, wB97, wB97X, wB97XD, LC-BLYP, CAM-B3LYP, LC-wPBE, LC-BLYP, LC-HCTH, LC-PBEPBE, LC-B97D, LC-M06L. All these TD-DFT calculations were carried out with Gaussian 09 package.

1.3 The Calculations of the Electronic Absorption Spectra

The conformational broadening[13,15,18] are considered in the calculation of absorption spectra. Then, for each conformation, the excitation energies are calculated

by using linear-response TDDFT approach at M06-2X/SVP level, and compared with the results at CAM-B3LYP, wb97XD, and BHandHLYP level (Figure S2). Although such treatment do not include nuclear quantum effects in the classical limit, quantum fluctuations of the nuclear skeleton are not obvious at relatively higher temperature. [16,17]

The S_0 to S_I (I>=1) absorption lineshape $F_I(v)$ is calculated according to

$$F_I(v) = \frac{1}{N_R}\sum_{R=1}^{N_R} f_I{}^R \delta\left(v_I{}^R - v\right) \qquad \text{(S1)}$$

Whereas, $F_I(v)$ is calculated as the average over N_R sample configurations from the values v_I^R and f_I^R determined for the electronic transition energy and the oscillator strength for one of the considered configurations ***R***. The total absorption spectra is given by the sum

$$f(v) = \sum_{I=1}^{N_I} F_I(v) \qquad \text{(S2)}$$

We used in place of the δ functions Gaussians having a half width at half-maximum (HWHM) of 1500 cm^{-1} (0.20 eV), and the N_R is the 20 lowest-lying transitions, which suffice for a complete characterization of the main absorption band.

1.5 The Static and Dynamic Analysis of the Imidazolium Rings

The possible interactions corresponding to the staked geometries of the imidazolium rings were further analyzed. Here, we use r and α to depict the stack orientation between two imidazolium rings, whereas, r is the offset distance from the geometric center of the second imidazolium ring to the normal vector of the first imidazolium ring, and α is the angle formed by the two normal vectors (Figure S6). Figure S6a shows the possibility of finding an imidazolium ring around another imidazolium ring with certain r andα, and all possible imidazolium rings stacking pairs were searched.

We can describe the microscopic dynamics of ILs with the rotational correlation function of the imidazolium rings

$$C(t) = \frac{1}{N}\sum_{i=1}^{N} \frac{3\cos^2 \alpha_i(t) - 1}{2} \qquad \text{(S3)}$$

$\alpha_i(t)$ is defined as the angle between the x axis (or z axis) at time zero and time t (see Figure S6b); *N* is the total number of imidazolium rings. The decorrelation of this angle with time gives insight into the rotational motion of the cation. And when the orientations of the imidazolium rings have no relationship, the function *C(t)* will decay to zero. The rotational time constant was obtained by integrating the function C(t) over times as[19]

$$\tau = \int_0^\infty C(t)dt \qquad \text{(S4)}$$

1.6 The QM/MM Calculations at ADC(2) and CC2 level.

We also tried to apply the QM/MM method to identify the solvent effects on single ion pair. The entire snapshot (~17408 atoms) from the dynamics trajectory is selected in the calculations. The QM region contain one ion pair and is treated at CC2/SVP and ADC(2)/SVP level as implemented in TURBOMOLE. The other ion pair is considered as MM point charges, which are derived from the same force field as MD simulations. Then, the single point calculations are performed to understand the excited state properties. The system is shown as follows. The red atoms are in the QM region, while the green ones are the MM atoms which are within ~2.5 Å from the QM atoms.

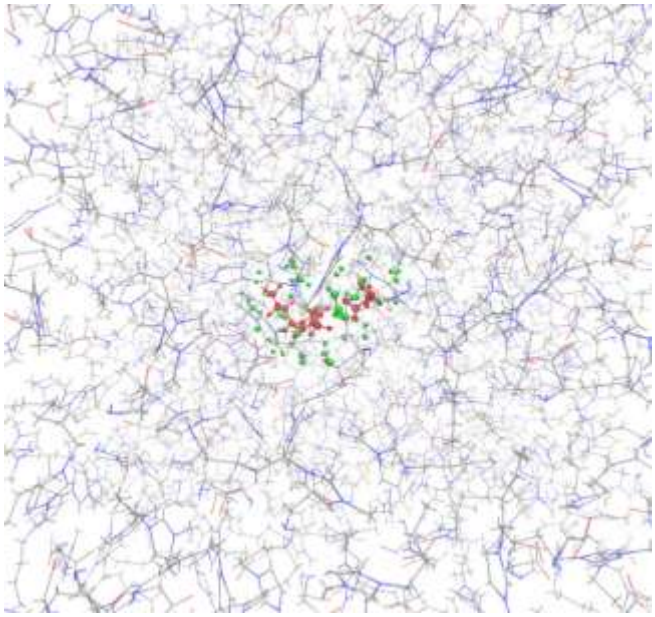

However, the QM/MM calculations were not trivial. Although there were no covalent bonds between QM/MM boundaries, the interaction among ion pairs are very strong, which cause close contact between QM atoms and MM atoms. For example, based on our statistical analysis, about 10~15 ions (cations or anions) were usually found within the range of 2.5 Å from the QM atoms. These ions are usually carry larger amount of charges, which could cause the overpolarization of the QM system.

In practice, for a randomly selected snapshot from the MD trajectory, the QM/MM calculations of single ion pair at CC2 or ADC(2) level often predict the excitation energy about ~1.5 eV higher than the single ion pair in gas phase. If we shift the MM charges within 2.5 Å from the QM region to partially avoid some overpolarization of the QM system, the predicted excitation energy would be about ~0.5 eV lower than the single ion pair in gas phase. This seems to be consistent with the results in the ion cluster model or the experimental observed non-negligible absorption band beyond 300 nm in bulk ionic liquid. Therefore, the calculated excitation energy seemed to be too sensitive to the position of the MM charge in ionic liquid. And we prefer to adopt the ion clusters model.

Rerference

1. Lopes, J. N. C.; Pádua, A. A. H. J. Phys. Chem. B 2006, 110(39), 19586-19592.
2. Jorgensen, W. L.; Maxwell, D. S.; Tirado-Rives, J. J. Am. Chem. Soc.1996, 118(45), 11225-11236.
3. Cornell, W. D.; Cieplak, P.; Bayly, C. I.; Gould, I. R.; Merz, K. M.; Ferguson, D. M.; Spellmeyer, D. C.; Fox, T.; Caldwell, J. W.; Kollman, P. A. J. Am. Chem. Soc. 1995, 117(19), 5179-5197.
4. Zhou, G.; Liu, X.; Zhang, S.; Yu, G.; He, H. J. Phys. Chem. B 2007, 111(25), 7078-7084.
5. Kagimoto, J.; Fukumoto, K.; Ohno, H. Chem. Commun. 2006(21), 2254-2256.
6. Fang, D.-W.; Guan, W.; Tong, J.; Wang, Z.-W.; Yang, J.-Z. J. Phys. Chem. B 2008, 112(25), 7499-7505.
7. Del Popolo, M. G.; Voth, G. A. J. Phys. Chem. B 2004, 108(5), 1744-1752.
8. Berendsen, H. J. C.; Postma, J. P. M.; Gunsteren, W. F. v.; DiNola, A.; Haak, J. R. J. Chem. Phys. 1984, 81(8), 3684-3690.
9. Darden, T.; York, D.; Pedersen, L. J. Chem. Phys. 1993, 98(12), 10089-10092.
10. Essmann, U.; Perera, L.; Berkowitz, M. L.; Darden, T.; Lee, H.; Pedersen, L. G. J. Chem. Phys. 1995, 103(19), 8577-8593.
11. Hess, B.; Bekker, H.; Berendsen, H. J. C.; Fraaije, J. G. E. M. J. Comput. Chem. 1997, 18(12), 1463-1472.

12. Van Der Spoel, D.; Lindahl, E.; Hess, B.; Groenhof, G.; Mark, A. E.; Berendsen, H. J. C. J. Comput. Chem. 2005, 26(16), 1701-1718.
13. Bernasconi, L.; Blumberger, J.; Sprik, M.; Vuilleumier, R. The J. Chem. Phys. 2004, 121(23), 11885-11899.
14. Xu, X.; Zheng, J.; Truhlar, D. G. J. Am. Chem. Soc. 2015, 137(25), 8026-8029.
15. Daku, L. M. L.; Linares, J.; Boillot, M.-L. Phys. Chem. Chem. Phys 2010, 12(23), 6107-6123.
16. Kresin, V. V. Phys. Rev. Lett. 1998, 81(25), 5702-5702.
17. Pacheco, J. M.; Schöne, W. D. Phys. Rev. Lett. 1998, 81(25), 5703-5703.
18. Marenich, A. V.; Cramer, C. J.; Truhlar, D. G. J. Phys. Chem. B 2015, 119(3), 958-967.
19. Cadena, C.; Maginn, E. J. *J. Phys. Chem. B* **2006**, *110*, 18026.

Figures and Tables

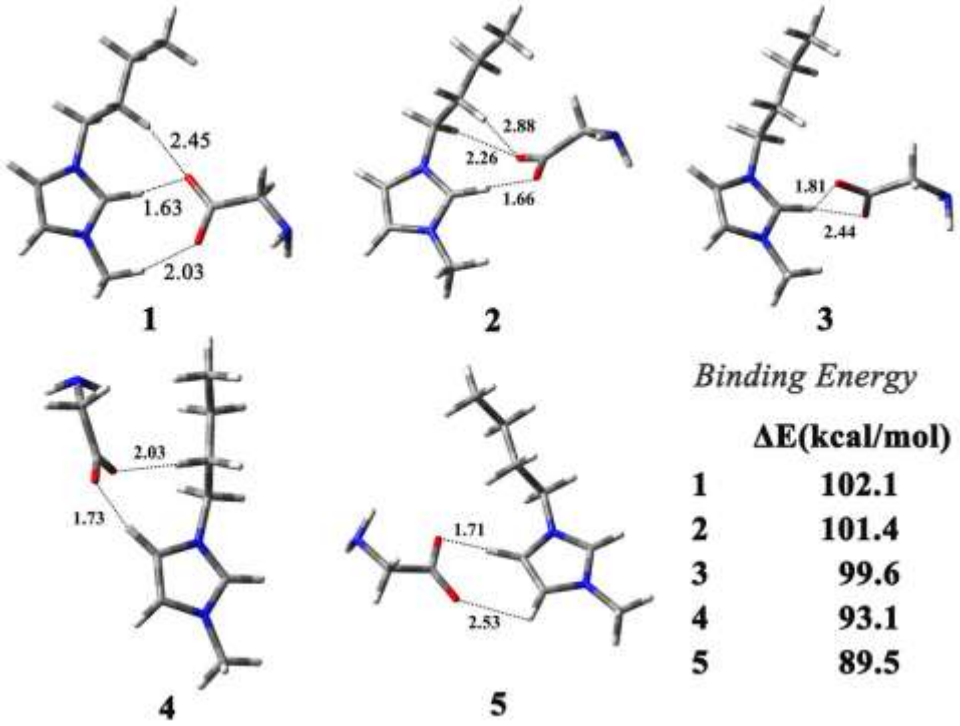

Figure S1 The optimized geometries of the single ion pair ([Bmim][Gly]) at B97D/cc-pVDZ level. The important hydrogen bond lengths (Å) were labeled, and the binding energies were calculated at MP2/CBS(3,4) level. The extrapolation at the complete basis set (CBS) limit of MP2 results can be carried out by the two point extrapolation scheme of Helgaker et al. (Chem. Phys. Lett. 1999, 302, 437)

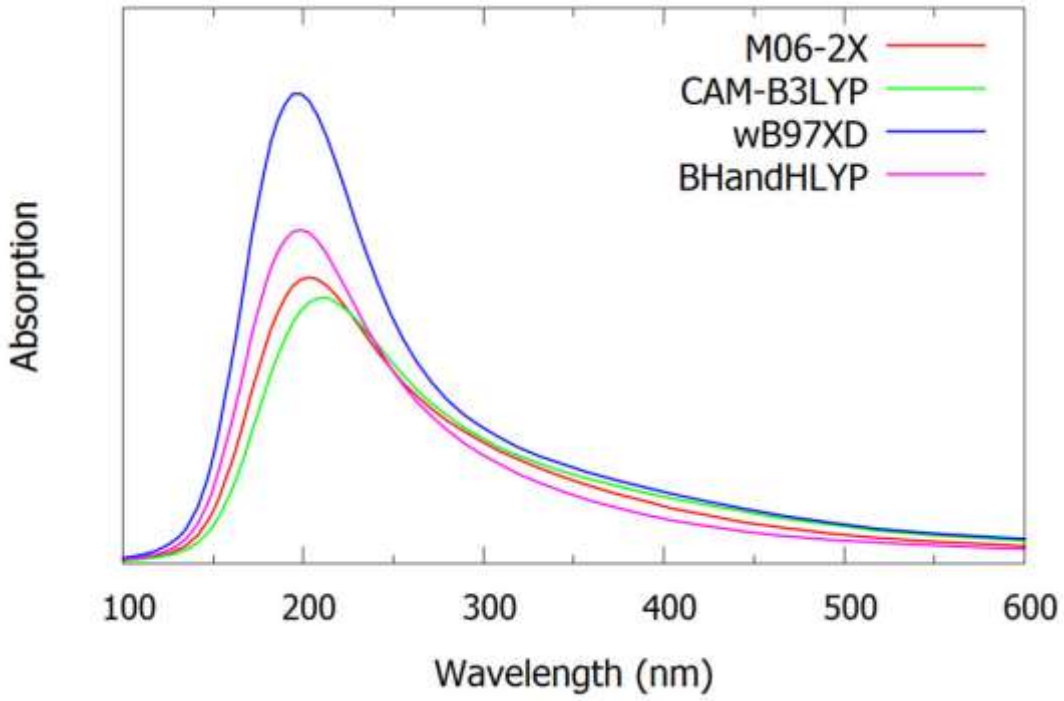

Figure S2 Absorption spectra of the free ion pairs sampled from MD trajectories, calculated at TDDFT/SVP level, with a few exchange-correlation functionals.

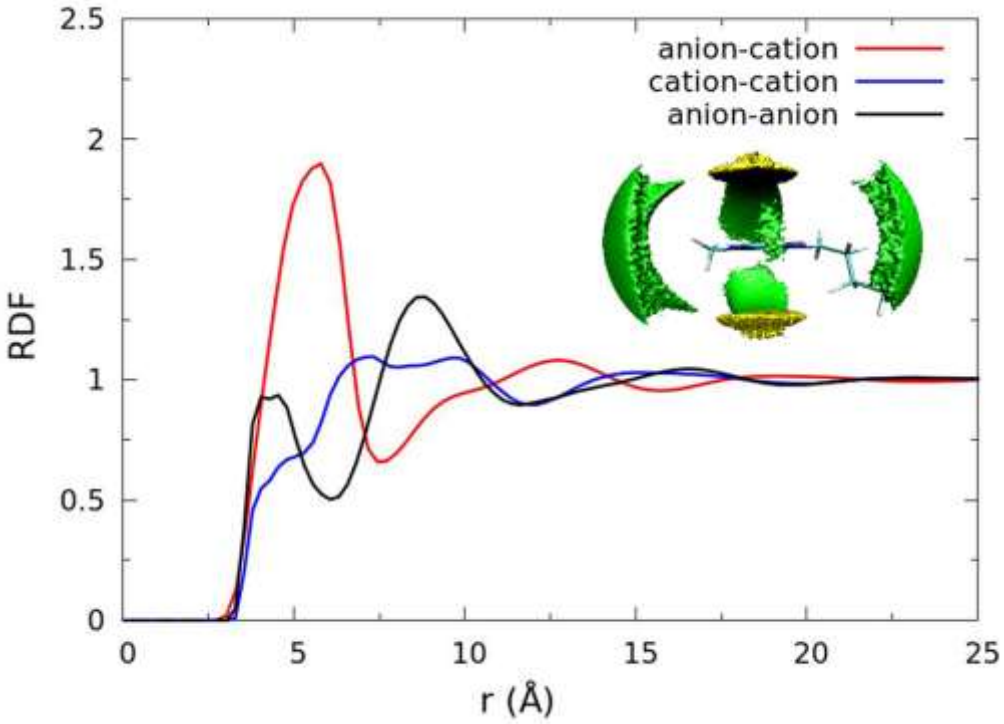

Figure S3 (a) Radial distribution functions (RDF) for the anion-cation, cation-cation and anion-anion in [Bmim][Gly]. (b) The absorption spectra with the static and dynamic method. Inset are the SDF of anions (green color) and cations (yellow color) around the cations for [Bmim][Gly]. Note that the geometric centers of the imidazolium ring and the central carbon in the amino acid anion were used in the calculations.

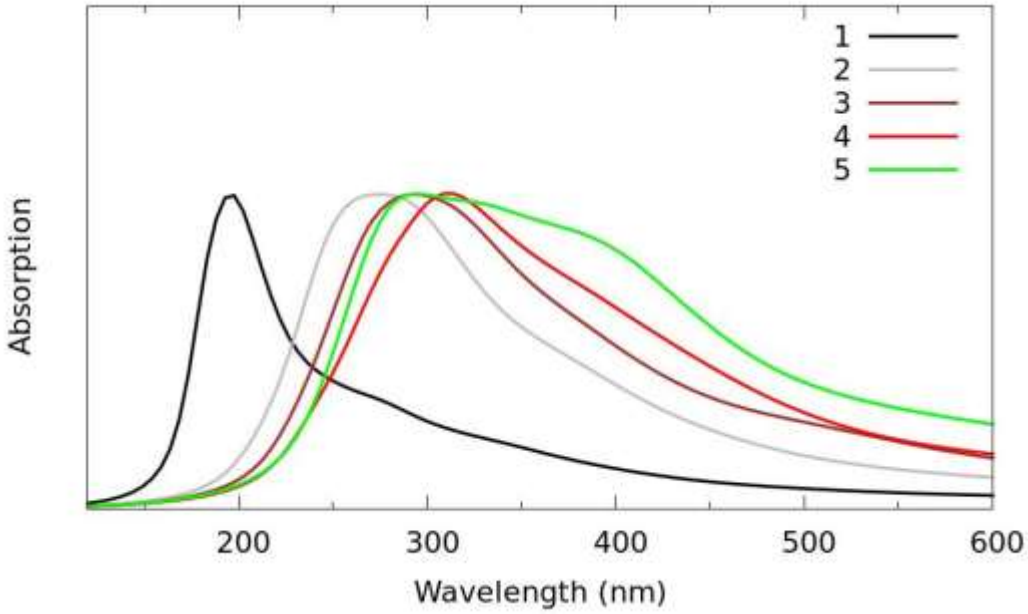

Figure S4 The absorption spectrum of the ion clusters *n*•([Bmim][Gly]) (*n*=1~5). The ion clusters (200 conformations) were obtained with ion number based sampling.

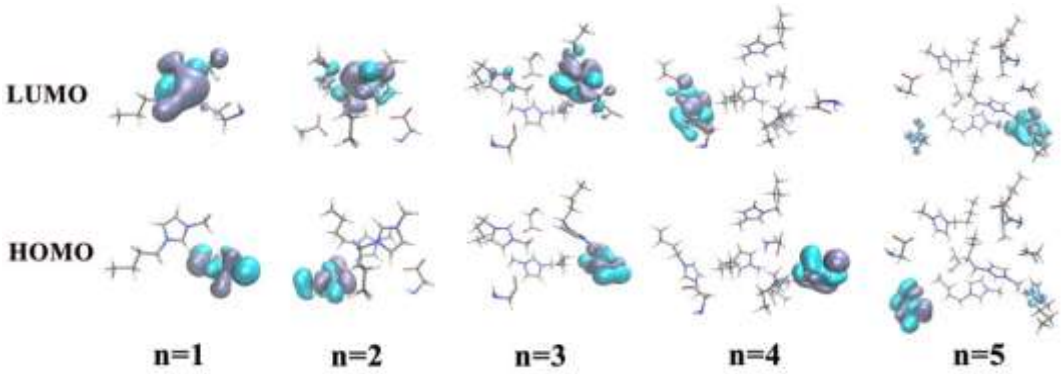

Figure S5 Molecular orbitals for typical geometries of *n*•([Bmim][Gly]) complexes

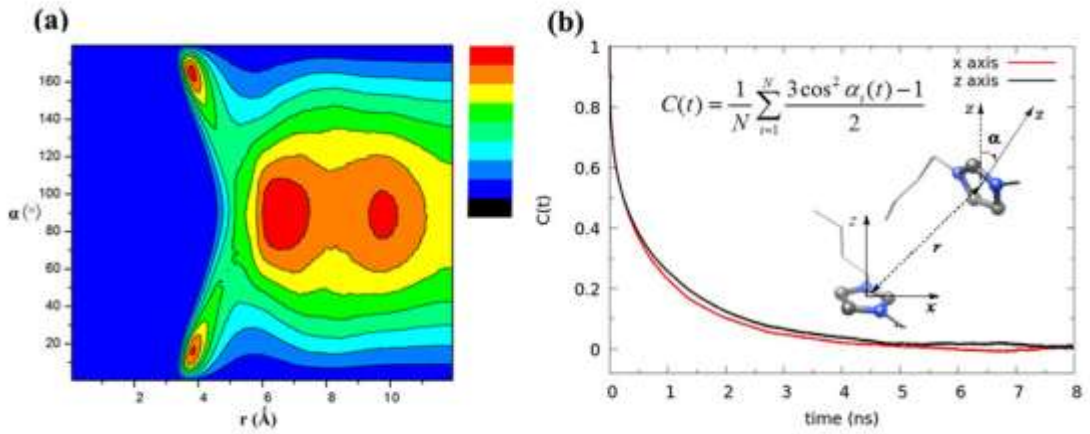

Figure S6 (a) Contours of the possible distributions of imidazolium rings around another imidazolium ring relative to r and α. (b) The rotational correlation function C(t) of the imidazolium ring along the *z* direction (the normal vector of the imidazolium ring) and the *x* direction (the plane of the imidazolium ring).

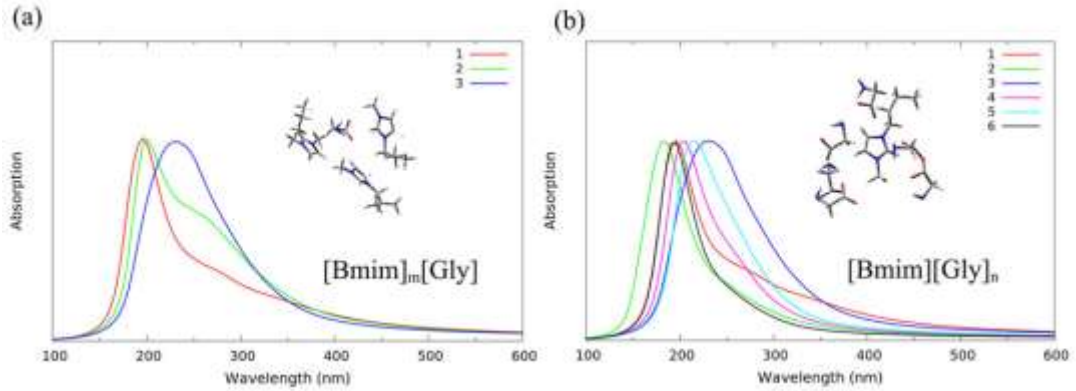

Figure S7 Absorption spectra of the charged ion clusters ($[Bmim]_m[Gly]_n$), namely, $[Bmim]_m[Gly]$ and [Bmim] $[Gly]_n$.

Table S1. The excitation energies calculated at CC2, ADC(2) level, and a few TD-DFT methods. The data were averaged over the optimized geometries (Figure S1) and the first ten excited states. The excitation energies were given in eV, and the standard derivations for the five optimized geometries were also given in the brackets.

Methods	**S_1**	**S_2**	**S_3**	**S_4**	**S_5**
CC2	4.71(0.29)	4.99(0.33)	5.45(0.31)	5.70(0.25)	5.88(0.23)
ADC(2)	4.62(0.29)	4.91(0.33)	5.31(0.31)	5.60(0.22)	5.80(0.20)
M062X	4.77(0.31)	5.28(0.29)	5.34(0.31)	5.58(0.25)	5.81(0.10)
M052X	4.88(0.32)	5.38(0.30)	5.49(0.29)	5.70(0.23)	5.91(0.12)
wB97XD	4.58(0.23)	4.93(0.23)	5.13(0.21)	5.51(0.40)	5.77(0.24)
CAM-B3LYP	4.51(0.31)	4.90(0.29)	5.08(0.29)	5.41(0.33)	5.74(0.23)
BHandHLYP	5.05(0.35)	5.52(0.35)	5.58(0.36)	5.96(0.25)	6.20(0.13)

Methods	**S_6**	**S_7**	**S_8**	**S_9**	**S_{10}**
CC2	6.15(0.14)	6.32(0.18)	6.48(0.29)	6.56(0.25)	6.77(0.31)
ADC(2)	6.06(0.21)	6.18(0.17)	6.42(0.30)	6.53(0.27)	6.72(0.31)
M062X	6.06(0.20)	6.23(0.31)	6.36(0.23)	6.61(0.26)	6.70(0.26)
M052X	6.13(0.18)	6.40(0.29)	6.52(0.27)	6.70(0.27)	6.82(0.30)
wB97XD	6.04(0.32)	6.19(0.22)	6.33(0.27)	6.58(0.24)	6.79(0.24)
CAM-B3LYP	5.98(0.29)	6.12(0.18)	6.23(0.21)	6.42(0.29)	6.50(0.28)
BHandHLYP	6.46(0.25)	6.53(0.28)	6.60(0.26)	6.71(0.25)	6.88(0.31)

Table S2. Statistical analysis for various theoretical methods with respect to the excitation energies of CC2 calculations; the first ten excited states were averaged with the optimized geometries (Figure S1).

Methods	RMSD (eV)	MSE (eV)	RE (%)
ADC(2)	0.11	0.10	2
M062X	0.17	-0.01	3
M052X	0.21	-0.13	4
B97XD	0.22	0.16	4
CAM-B3LYP	0.25	0.22	5
HandHLYP	0.35	-0.32	7
BMK	0.39	0.36	7
wB97X	0.47	-0.41	10
HISSbPBE	0.59	0.56	12
M11	0.62	-0.55	13
LC-wPBE	0.70	-0.63	14
wB97	0.74	-0.68	15
LC-BLYP	1.01	-0.97	20
LC-HCTH	1.02	-0.97	21
LC-PBEPBE	1.04	-1.00	21
LC-B97D	1.05	-1.01	21
LC-M06L	1.08	-1.03	22
LC-N12	1.13	-1.09	23
N12SX	1.16	1.14	22
M06HF	1.18	-1.12	22
B1B95	1.25	1.24	24
PW1PBE	1.32	1.31	25
PW1PW91	1.32	1.31	25
PBE1PBE	1.34	1.33	26

M06	1.40	1.39	27
M05	1.45	1.43	28
HSE2PBE	1.48	1.46	28
SEH1PBE	1.50	1.48	29
HSE1PBE	1.50	1.48	29
X3LYP	1.56	1.55	30
N12SX	1.57	1.55	30
B3P86	1.64	1.63	31
B3PW91	1.66	1.65	32
PW3PBE	1.66	1.65	32
B3LYP	1.68	1.67	32
MN12L	1.94	1.92	37
tHCTHhyb	1.95	1.94	37
TD-HF	2.13	-2.11	41
TPSSh	2.14	2.13	41
CIS	2.31	-2.30	44
LC-M11L	2.38	2.37	46
M11L	2.38	2.37	46
M06L	2.57	2.56	49
VSXC	2.76	2.75	53
TPSSTPSS	2.78	2.76	53
tHCTH	2.87	2.86	55
B97D	2.91	2.90	56
B97D3	2.91	2.90	56
N12	2.94	2.93	56
SVWN	2.97	2.96	57
W91PW91	2.99	2.98	57
HCTH407	2.99	2.98	57
OLYP	2.99	2.98	57

PBEPBE	3.00	2.99	57
BLYP	3.01	2.99	57

*RMSD, root of mean square derivation; MSE, mean signed error; RE (%), relative error.